Characterization and Application of Nanomaterials (2022) Volume 5 Issue 1
doi:10.24294/can.v5i1.1408

ORIGINAL RESEARCH ARTICLE

Synthesis and *in Vitro* anticancer properties of $Cu_{2-x}Se$–AIPH nanomaterials

Juan Lu, Yini Mao, Jun Yang*

School of Chemistry and Chemical Engineering, Southwest University, Chongqing 400715, China. E-mail: jyang@swu.edu.cn

ABSTRACT

The $Cu_{2-x}Se$ nanoparticles were synthesized by high temperature pyrolysis, modified with aminated polyethylene glycol in aqueous solution and loaded with compound 2,2′–azobis[2–(2–imidazolin–2–yl)propane] dihydrochloride (AIPH). The obtained nanomaterials can induce photothermal effect and use heat to promote the generation of toxic AIPH radicals under the irradiation of near-infrared laser (808 nm), which can effectively kill cancer cells. A series of *in vitro* experiments can preliminarily prove that $Cu_{2-x}Se$–AIPH nanomaterials have strong photothermal conversion ability, good biocompatibility and anticancer properties.

Keywords: $Cu_{2-x}Se$ Nanoparticles; AIPH; Photothermal Effect; Anticancer Properties

ARTICLE INFO

Received: 26 September 2021
Accepted: 19 November 2021
Available online: 30 November 2021

1. Introduction

Cancer has now become one of the major threats to people's health all over the world, and countless people lose their lives due to cancer every year. However, there are problems lying in treatment methods of traditional chemotherapy, radiotherapy, and surgery, such as great side effects and low treatment efficiency. Therefore, it is urgent to develop some novel and effective cancer treatment methods[1–5]. In recent years, photothermal therapy (PTT) has attracted more and more scientists' attention in the field of cancer treatment due to its low invasiveness[6–8]. The therapeutic principle is that photothermal materials can effectively convert light energy into heat energy after absorbing the external light energy, thereby triggering the withering or death of cancer cells. Based on this, batches of excellent photothermal materials have been created continuously, including binary chalcogenides with unique physical and chemical properties[9]. At the same time, near-infrared light is also closely connected to cancer treatment due to its deeper penetration depth in biological tissues compared with ultraviolet light[10–12].

Take advantage of the photothermal effect of selenide $Cu_{2-x}Se$ and combine it with other therapeutic agents. $Cu_{2-x}Se$ nanoparticles with a particle size of 20–40 nm were synthesized by a classical high-temperature pyrolysis method, and the compound 2,2′–azobis[2–(2–imidazoline–2–yl)propane] dihydrochloride (AIPH), an azo compound that rapidly decomposes during heating to produce toxic alkyl groups, was loaded after aminated polyethylene glycol modification.

Due to the large tumor cell gap, the tumor microenvironment has high enhanced permeability and retention effect (EPR), and anti-tumor nanomaterials will passively be targeted to tumor sites to play a role of treatment; without extra light and heating, the body temperature about 37 ℃ will not cause the decomposition of AIPH to generate free radicals. Therefore, AIPH itself will not cause damage to the normal tissues of the organism. Due to the lack of copper atoms, $Cu_{2-x}Se$ nanoparticles have strong plasmon resonance absorption (LSPR) and excellent photothermal properties in the near-infrared region where the penetration of biological tissues is strong, and have been increasingly used in the field of photothermal therapy. The $Cu_{2-x}Se$–AIPH nanoparticles synthesized by this system can generate photothermal temperature up to 48 ℃ after absorbing 808 nm near-infrared light, which is sufficient for photothermal therapy. Under the action of near-infrared light, the photothermal effect of $Cu_{2-x}Se$ nanoparticles can play a synergistic effect with AIPH free radicals to kill tumor cells. The anticancer properties of $Cu_{2-x}Se$–AIPH materials were preliminarily proved through a series of *in vitro* experiments.

2. Experiment

2.1 Experimental reagents

The reagents used in this experiment including cuprous chloride (CuCl), aminated polyethylene glycol (NH_2–PEG(2000)–NH_2), 1–(3–dimethylaminopropyl)–3–ethylcarbodiimide hydrochloride (EDC), N–hydroxysuccinimide (NHS), oleylamine, octadecene, and anhydrous ethanol (C_2H_5OH) were all at an analytical grade and were used directly in the experimental process without further purification. All chemicals were purchased from Sigma-Aldrich, except for the selenium powder (Se) which was purchased from Sinopharm Chemical Reagent Co., Ltd.

2.2 Preparation process

$Cu_{2-x}Se$ nanoparticles were synthesized by a typical solvent injection method with slight modifications from the previous literature[13]. The preparation process was mainly divided into two stages. First, the precursor of Se–OAm (selenium-oleylamine) was synthesized. Weigh 10 mmol of selenium powder and 10 mL of oleylamine into a three-necked flask, set up a pyrolysis device, add nitrogen, and heat it to 140 ℃ with a heating mantle for 10 min to remove moisture and some low-boiling impurities. Then the temperature was raised to 320 ℃ for a period of time, and the obtained brown solution was the precursor Se–OAm. At the same time of the constant temperature reaction, take another four-necked bottle, weigh 0.5 mmol of CuCl, 8 mL of octadecene (ODE) and 2 mL of oleyl amine in it, also keep it in a nitrogen environment for 10 min, and then heat it up to 200 ℃ and immediately inject the Se–OAm solution prepared in the previous step, and then continue to heat it up to 220 ℃ for a period of time. The obtained black-brown solution was washed three times alternately with ethanol, cyclohexane and ethanol to obtain $Cu_{2-x}Se$ nanoparticles, wherein the amount of each washing solvent was equal to the volume of the reaction solution, about 10 mL. The synthesized $Cu_{2-x}Se$ nanoparticles were then modified with amino groups to improve their hydrophilicity for subsequent compound loading and testing applications. The prepared nanoparticles were mixed with 10 mg of EDS and 20 mg of NHS in methanol solvent and stirred for 1.5 h in the dark environment. Then 40 mg of NH_2–PEG(2000)–NH_2 was added to the above solution, and the obtained solution was washed with methanol and deionized water and centrifuged after the reaction was continued for 12 h. Subsequently, 0.2 g of AIPH and the aminated product were kept in a water bath at 70 ℃ for 4 h. Finally, the reactant was washed several times with ethanol to remove excess AIPH, and the precipitate was collected[14].

2.3 Characterization of properties

Phase analysis was performed using a Rigaku D/max–TTR–III diffractometer (Cu–Kα radiation λ = 0.15405 nm), the scanning range 2θ = 10°–90°, 10°/min of the scanning speed; a FEI Tecnai G^2S–Twin transmission electron microscope was used to observe the morphology (the sample was first dispersed in cyclohexane or ethanol solvent, and then dropped on a carbon support film for observation

after the solvent was volatilized); confocal laser scanning microscope observation was performed on a Leica SP8 device (CLSM); X-ray electron spectroscopy (XPS) measurements were performed using a surface analysis system (Thermofisher Escalab Xi+) with AlKα radiation ($h\nu$ = 1486.6 eV) from a monochromatic X-ray source and a spot size of 500 μm. The above characterizations were all done at room temperature.

3. Results and discussion

3.1 Morphology, phase and elemental analysis

Figure 1(a) is the XRD pattern of the product synthesized by the high temperature pyrolysis method in the first step. It can be seen that the XRD pattern of the product shows the position and relative intensity of the main characteristic peaks, which are consistent with the standard pattern of $Cu_{2-x}Se$ (JCPDS No.06–0680), proving the successful synthesis of $Cu_{2-x}Se$ crystals with good crystallinity.

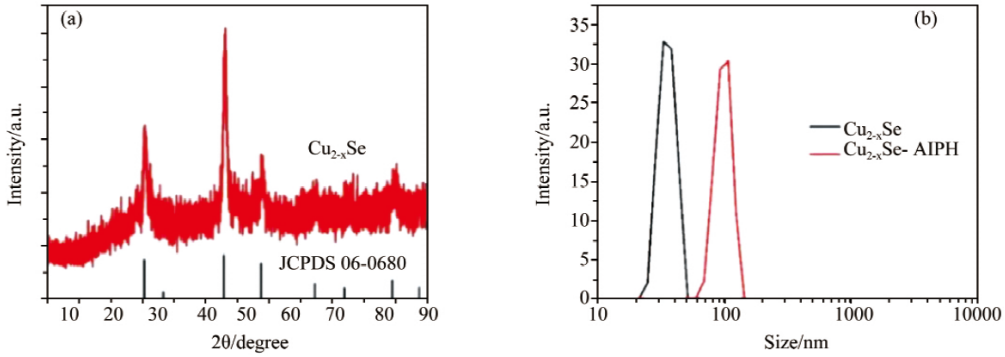

Figure 1. (a) XRD pattern of $Cu_{2-x}Se$ nanoparticles; **(b)** dynamic light scattering particle size distribution of $Cu_{2-x}Se$ and $Cu_{2-x}Se$–AIPH nanoparticles.

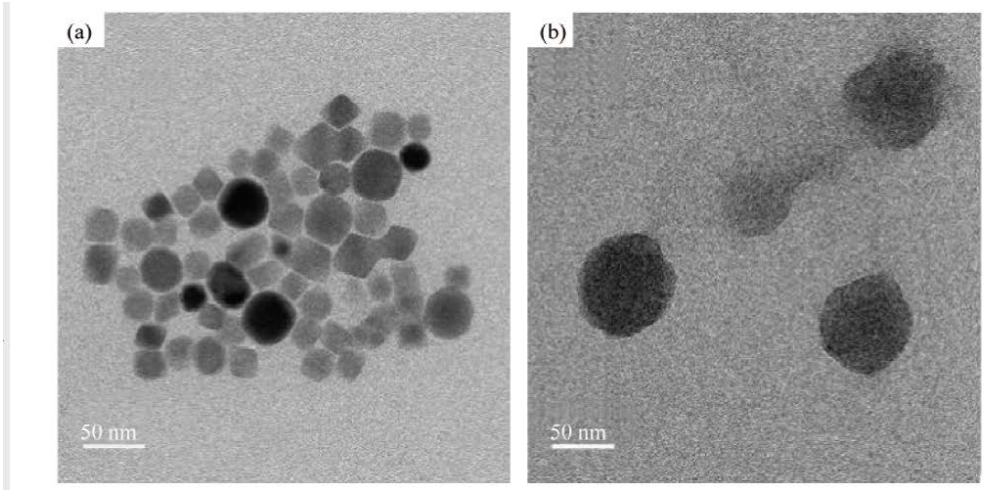

Figure 2. (a) TEM of $Cu_{2-x}Se$ nanoparticles; **(b)** TEM of $Cu_{2-x}Se$–AIPH nanoparticles.

Figure 2 shows the morphology of $Cu_{2-x}Se$ and $Cu_{2-x}Se$–AIPH nanoparticles. It can be clearly seen from **Figure 2(a)** that the particle size of $Cu_{2-x}Se$ nanoparticles prepared by high temperature pyrolysis is 20–40 nm, and the morphology is mostly square or spherical with clearly visible outline. After transferring water and loading AIPH, it can be seen from **Figure 2(b)** that the particle size increases to about 80 nm, and the morphology changes to a single spherical shape. It can be concluded that the increase in the particle size of nanoparticles may be due to the coagulation of the oily $Cu_{2-x}Se$ nanoparticles in the subsequent reaction process of the aqueous solution. The mapping images of Cu, Se, C, N, and O elements in **Figure 3** further verify the successful synthesis of the product. **Figure 1(b)** shows the dynamic light scattering particle size distribution of $Cu_{2-x}Se$ and $Cu_{2-x}Se$–AIPH. It can be seen from the figure that the particle size of the particles is basically the same as the

value in the previous transmission diagram.

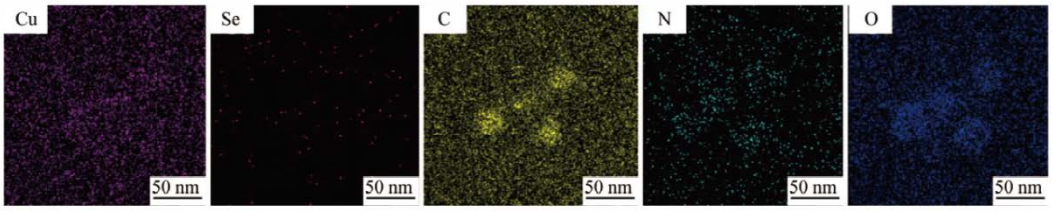

Figure 3. Elemental mapping images of $Cu_{2-x}Se$–AIPH nanoparticles.

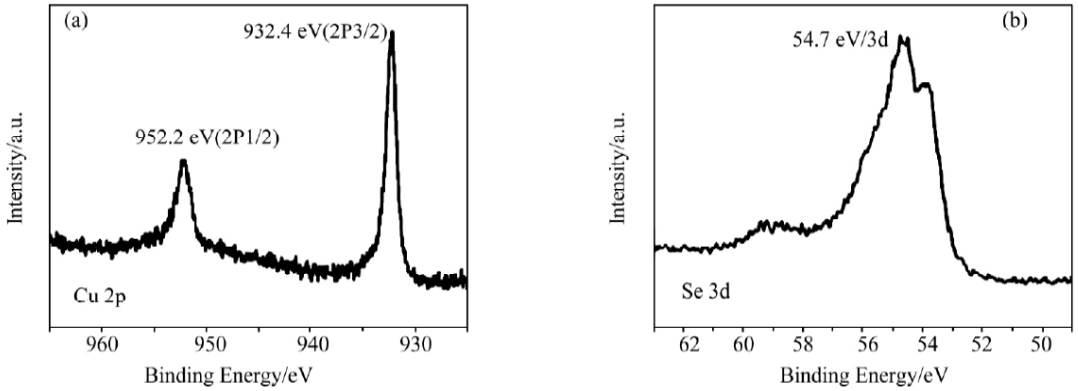

Figure 4. XPS spectra of Cu 2p **(a)** and Se 3d **(b)** in $Cu_{2-x}Se$–AIPH nanoparticles.

Figure 4 is the XPS spectrum of Cu and Se elements in $Cu_{2-x}Se$–AIPH nanoparticles. Specifically, the binding energy of the characteristic peaks of Cu 2p in **Figure 4(a)** is 952.2 eV and 932.4 eV, proving the existence of monovalent copper in the material; the binding energy of the characteristic peaks of Se 3d in **Figure 4(b)** is 54.7 eV, which proves that selenium in the material is negative divalent. The change of Zeta potential during the reaction also confirmed the progress of each step of the reaction. **Figure 5(a)** is the Zeta potential change diagram of each step of the reaction product aqueous solution ($Cu_{2-x}Se$, NH_2–$Cu_{2-x}Se$, $Cu_{2-x}Se$–AIPH). It can be seen that the potential of the initial $Cu_{2-x}Se$ particle solution was –10.35 mV, which increased significantly after the introduction of amino groups (–1.3 mV). The potential was further increased to 16 mV. The value of Zeta potential can reflect the stability of the system to some extent. The lower the Zeta potential value (positive or negative) is, when the attractive force exceeds the repulsive force, the more likely the nanoparticles in the system are to agglomerate. Therefore, combined with the change of the Zeta potential value, the change of the particle size and morphology in the transmission image can be explained to a certain extent. At the beginning, the potential of the $Cu_{2-x}Se$ particle solution was –10.35 mV, and the particles began to have a tendency to coagulate, but it was relatively stable; after the amino group was modified in the aqueous solution, the potential of the material became –1.3 mV, and the negative value of Zeta potential became lower , the system began to become unstable, and the particles will coagulate to a certain extent; finally, the Zeta potential of the $Cu_{2-x}Se$–AIPH material became 16 mV, the positive value of Zeta potential was higher, and the system gradually tended to be stable. After the square or spherical $Cu_{2-x}Se$ particles coagulated in the solution, the particle size of the final material increased and the morphology changed to a single spherical shape.

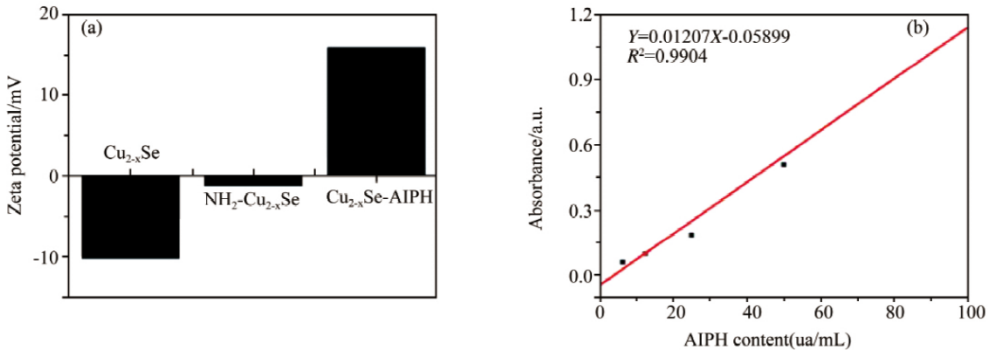

Figure 5. (a) Zeta potential change diagram of products of each step in the reaction process; **(b)** standard absorption curve of AIPH.

Figure 5(b) is the standard curve of the supported compound AIPH. From the figure, the linear relationship between the concentration (X) of AIPH and its UV-Vis absorbance (Y) can be obtained: $Y = 0.01207X - 0.05899$. **Figure 6(a)** is the UV-Vis absorption curve of the $Cu_{2-x}Se$ material before and after loaded with AIPH. It can be seen that, compared with the absorption curve of $Cu_{2-x}Se$ nanoparticles, that of $Cu_{2-x}Se$–AIPH appeared at 360 nm. The characteristic absorption peaks of AIPH proved the successful loading of AIPH. Combined with the linear relationship obtained from the AIPH standard curve, the loading of AIPH can be calculated to be 8.1%. To verify the generation of AIPH radicals, 1 mg/mL 2,2′–azobis(3–ethylbenzothiazoline–6–sulfonic acid) (ABTS) and $Cu_{2-x}Se$–AIPH of the same concentration were mixed and reacted for 2 h in a water bath at 45 ℃, and the UV-Vis absorption spectrum of the reaction solution was measured. **Figure 6(b)** is the characteristic absorption curve of the reaction product ABTS, indicating that AIPH decomposes to generate free radicals under the heating condition of 45 ℃, which further react with ABTS to generate ABTS free radicals.

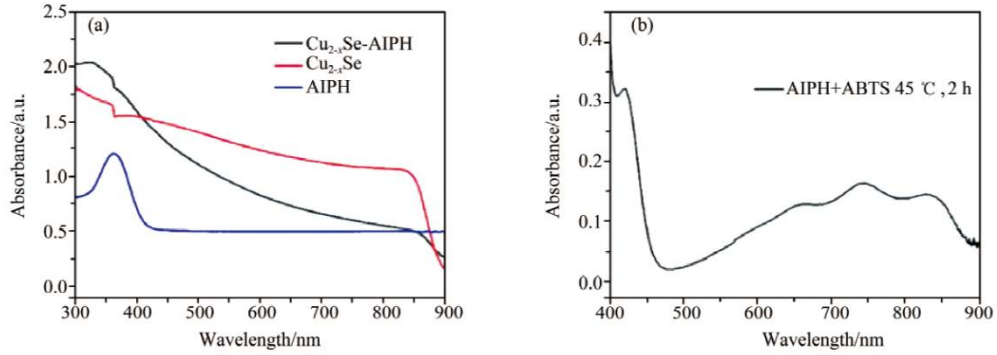

Figure 6. (a) UV-Vis absorption curves of $Cu_{2-x}Se$, $Cu_{2-x}Se$–AIPH and AIPH; **(b)** the reaction curve of AIPH and ABTS when heated at 45 ℃.

3.2 Photothermal conversion performance

Since the photothermal effect of nanoparticles plays a key role in the subsequent treatment of tumor cells, the related photothermal properties of synthetic materials were first explored in aqueous solution[15–17]. The temperature curves of $Cu_{2-x}Se$, $Cu_{2-x}Se$–AIPH solution and solvent water recorded by an infrared thermal imager under the irradiation of near-infrared light (808 nm) are shown in **Figure 7(a).** It can be clearly seen that the temperature of the solvent water basically fluctuates around room temperature, while the temperature of $Cu_{2-x}Se$ and $Cu_{2-x}Se$–AIPH materials increases significantly under the irradiation of 808 nm laser, which preliminarily proves the photothermal conversion properties of the materials. Moreover, the temperature of the material can reach 48 ℃ or above in a short period of 5 min, meeting the temperature requirements for the treatment of cancer cells *in vitro* and *in vivo*. The subsequent connection of amino groups and loading of AIPH may block the absorption of near-infrared light by the photothermal agent $Cu_{2-x}Se$ to a certain extent, but happily, on the contrast, the temperature

rise rate of $Cu_{2-x}Se$–AIPH nanoparticles every 50 s and the final stable temperature value only decrease slightly, which does not affect the performance and application of the material[18].

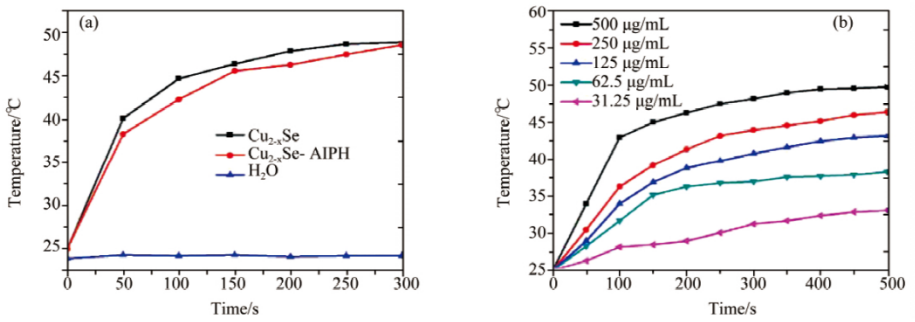

Figure 7. (a) Heating curves of $Cu_{2-x}Se$, $Cu_{2-x}Se$–AIPH solution and water under 808 nm laser irradiation; **(b)** temperature variation curves of $Cu_{2-x}Se$–AIPH solution with different concentrations under 808 nm laser irradiation. All laser power is 1 W/cm^2.

Then, the temperature changes of $Cu_{2-x}Se$–AIPH solutions with different concentrations (31.25, 62.5, 125, 250, 500 μg/mL) during the irradiation time of 500 s were further explored. It can be seen from **Figure 7(b)** that the temperature of each group of solutions increases regularly with the prolongation of infrared light irradiation time and the greater the concentration, the faster the temperature rises. When the material's concentration is 31.25 μg/mL, the heating rate is the smallest, and the final stable temperature is only about 33 ℃, which is lower than the normal temperature of the human body; when the material's concentration is 500 μg/mL, the heating rate is the largest, and the final stable temperature can reach around 48 ℃, which is enough to induce apoptosis and death of cancer cells[19,20].

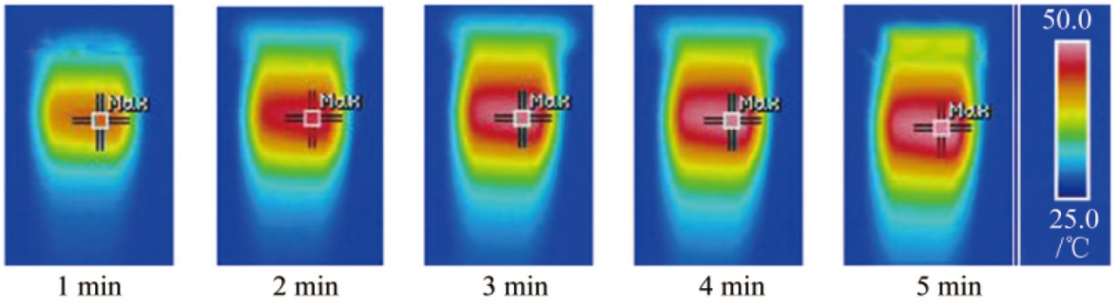

Figure 8. Infrared thermal images of the $Cu_{2-x}Se$–AIPH material (500 μg/mL).

In order to observe the photothermal effect of the $Cu_{2-x}Se$–AIPH material more intuitively, we used an infrared thermal imager to record the every-minute infrared thermal imaging pictures of 500 μg/mL material when the material was irradiated by 808 nm laser for 5 min. It can be seen from **Figure 8** that with the extension of time, the color of the thermal imaging picture of the material gradually changes from light yellow to dark red to white-hot. It can be determined that the material can generate a large amount of heat after absorbing near-infrared light, causing a significant increase of the solution temperature. Compared with the standard temperature bar, it can be roughly judged that the final photothermal temperature of the material can reach about 48 ℃. The above tests show that $Cu_{2-x}Se$–AIPH nanomaterials can effectively convert near-infrared light into thermal energy, and thus have the potential for photothermal therapy.

3.3 Anticancer properties in vitro

Before carrying out biological experiments, the biocompatibility of the materials must be effectively evaluated to avoid unnecessary side effects to the organism[21]. After co-culturing $Cu_{2-x}Se$–AIPH materials of different concentrations (15.6, 31.3, 62.5, 125, 250, 500 μg/mL) with L929 fibroblasts for 24 h, the cell biocompatibility was evaluated by MTT analysis. **Figure 9(a)** shows the state of cells after cultured with different concentrations of $Cu_{2-x}Se$–AIPH nanomaterials. It can be seen that even

when the material's concentration is as high as 500 μg/mL, the cell viability is still as high as 85%, which preliminarily proves $Cu_{2-x}Se$–AIPH nanomaterials have good biocompatibility.

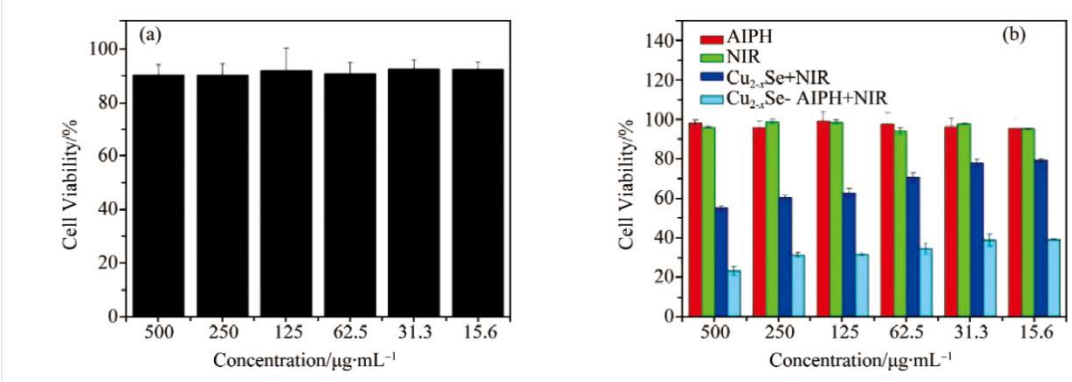

Figure 9. (a) Biocompatibility of $Cu_{2-x}Se$–AIPH nanomaterials with different concentrations; **(b)** cytotoxicity of $Cu_{2-x}Se$ and $Cu_{2-x}Se$–AIPH nanoparticles with different concentrations to HeLa cells.

Next, the cytotoxicity of nanoparticles to HeLa cells was analyzed by a similar MTT method. **Figure 9(b)** is a histogram of the viability of HeLa cells cultured for the same time under different conditions. As shown in the figure, the cells were divided into four groups, namely: AIPH, NIR, $Cu_{2-x}Se$+NIR, $Cu_{2-x}Se$–AIPH+NIR. It can be seen from the figure that the survival rate of cells in all AIPH and NIR groups can reach more than 95%, which proves that AIPH culture alone or infrared light irradiation has basically no effect on cells. The cell viability of the $Cu_{2-x}Se$+NIR group dropped to about 50% (with a concentration of 500 μg/mL), which was attributed to the good photothermal properties of $Cu_{2-x}Se$ nanoparticles under the action of near-infrared light, while the cell viability of $Cu_{2-x}Se$–AIPH+NIR group can be reduced to 20% (with a concentration of 500 μg/mL). It can be seen from the analysis that this is because compared with $Cu_{2-x}Se$+NIR, AIPH in the $Cu_{2-x}Se$–AIPH material can also be decomposed into free radicals under the photothermal action of $Cu_{2-x}Se$, and the synergistic effect of the two further enhances the ability of the system to kill cancer cells[22,23].

In order to illustrate the above cytotoxic results more intuitively, a staining experiment was performed using propidium iodide (PI) (this staining method can only mark dead cells with red)[24,25]. **Figure 10** shows the CLSM images of HeLa cells under different incubation conditions. After similar incubation in the cytotoxicity experiment, similar results were obtained in the staining experiment, namely: in the AIPH and NIR groups, the number of dead red cells was the least; the number of dead red cells in $Cu_{2-x}Se$–AIPH+NIR was the highest, i.e., the treatment effect was the best, followed by $Cu_{2-x}Se$+NIR. In conclusion, the above cell experiments can preliminarily prove that the $Cu_{2-x}Se$–AIPH material has good biocompatibility and anticancer properties[26].

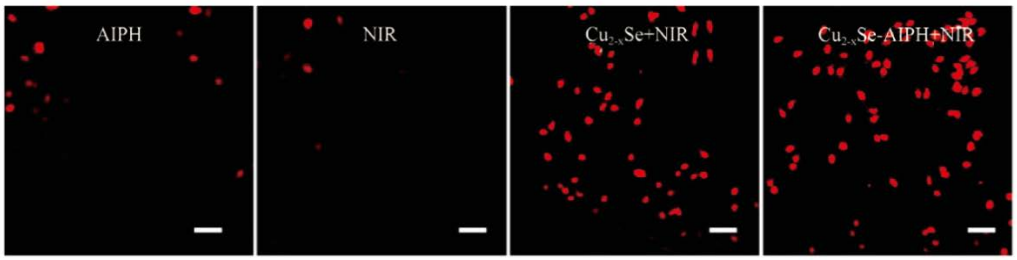

Figure 10. CLSM images of HeLa cells incubated under different conditions (the scale bar of all images is 100 μm).

4. Conclusion

In summary, a series of experiments have proved that the photothermal conversion temperature of the constructed $Cu_{2-x}Se$–AIPH system is as high as 48 °C, which can be used for photothermal therapy; *in vitro* cell experiments prove that the biocompatibility of the material is better, and the cell

survival rate is as high as 85%, when the material concentration is 500 μg/mL; the survival rate of cancer cells in the $Cu_{2-x}Se$–AIPH+NIR group could be reduced to 20%, when the material concentration was 500 μg/mL. The above work shows that the $Cu_{2-x}Se$–AIPH material has the potential for tumor therapy and can be further developed for biological applications.

Conflict of interest

The authors declare that they have no conflict of interest.

Acknowledgements

National Natural Science Foundation of China (51302229).

References

1. Sun Y, Zhou Q, Su S. Research progress of Chinese medicine compatibility in cancer treatment (in Chinese). World Journal of Integrated Traditional and Western Medicine 2015; 10(10): 1476–1480.
2. Chen W, Liu Y, Wang S, *et al.* Research progress in co-delivery of gene and chemotherapy drugs with cationic liposome carrier for cancer therapy. Acta Pharmaceutica Sinica 2012; 47(8): 986–992.
3. Jiang Y, Liu S, Zhang Y, *et al.* Magnetic mesoporous nanospheres anchored with LyP–1 as an efficient pancreatic cancer probe. Biomaterials 2017; 115: 9–18.
4. Liu J, Yang Y, Zhu W, *et al.* Nanoscale metal-organic frameworks for combined photodynamic & radiation therapy in cancer treatment. Biomaterials 2016; 97: 1–9.
5. Zhao T, Wang P, Li Q, *et al.* Near-infrared triggered decomposition of nanocapsules with high tumor accumulation and stimuli responsive fast elimination. Angewandte Chemie International Edition 2018; 57(10): 2611–2615.
6. Zhao C, Li W. Progress in inorganic nanomaterials for photothermal therapy of cancer. Tumor 2017; 37(3): 289–294.
7. Zhang X, Li W. Progress in nanomaterials for photothermal therapy in cancer. Chinese Journal of Pharmaceuticals 2016; 47(8): 1065–1069.
8. Zhao M, Ding J, Mao Q, *et al.* A novel $\alpha_v\beta_3$ integrin-targeted NIR–II nanoprobe for multimodal imaging-guided photothermal therapy of tumors *in vivo*. Nanoscale 2020; 12(13): 6953–6958.
9. Feng F, Feng J, Wu C, *et al.* Chemical synthesis and assembly of quasi-two-dimensional metal chalcogenides graphene analogues. Scientia Sinica (Chimica) 2012; 42(11): 1575–1585.
10. Rui X, Yao X, An L, *et al.* Recent advances of theranotics agents based on copper chalcogenide. Journal of Shanghai Normal University (Natural Sciences) 2016; 45(6): 748–756.
11. Cai X, Shang Y, Wang C. Application of mesoporous nano-silica as drug carrier in cancer therapy. Chinese Journal of Biochemistry and Molecular Biology 2019; 35(3): 274–279.
12. Jiang W, Chen J, Gong C, *et al.* Intravenous delivery of enzalutamide based on high drug loading multifunctional graphene oxide nano-particles for castration-resistant prostate cancer therapy. Journal of Nanobiotechnology 2020; 18(1): 50.
13. Liu Y, Zhu D, Hu Y, *et al.* Controlled synthesis of $Cu_{2-x}Se$ nanoparticles as near-infrared photothermal agents and irradiation wave-length dependence of their photothermal conversion efficiency. Langmuir 2018; 34(46): 13905–13909.
14. Yan Y, Qian X, Yin J, *et al.* Preparation and characterization of $Cu_{2-x}Se$ nanocrystals by trisodium citrate-assisted photochemical route. Chinese Journal of Inorganic Chemistry 2003; (10): 1133–1136.
15. Tao C, Yang G, Yang S. The research progress in $Fe@Fe_3O_4$ based diagnosis and treatment platform. Journal of Shanghai Normal University (Natural Sciences) 2019; 48(4): 449–459.
16. Jiao T, Huang X, Zhang L, *et al.* Research progress on syntheses of nanomaterials based on photothermal agent/photosensitizer and applications. Journal of Yanshan University 2017; 41(3): 189–203.
17. Jiang X, Zhang S, Ren F, *et al.* Ultrasmall magnetic $CuFeSe_2$ ternary nanocrystals for multimodal imaging guided photothermal therapy of cancer. ACS Nano 2017; 11(6): 5633–5645.
18. Zhu Y, Huang K, Wang Y, *et al.* Advance on HDAC multi-target inhibitors in the treatment of cancer. Journal of Liaocheng University (Natural Science

Edition) 2019; 32(5): 71–79.
19. Ming C, Chen H, Pei M. Researches on luminescent thermal properties of Er^{3+}/Yb^{3+}-doped YAG crystal for optical temperature sensor. Journal of Liaocheng University (Natural Science Edition) 2020; 33(2): 73–77.
20. Pan W, Dai C, Li Y, *et al.* PRP-chitosan thermoresponsive hydrogel combined with black phosphorus nanosheets as injectable biomaterial for biotherapy and phototherapy treatment of rheumatoid arthritis. Biomaraterials 2020; 239: 119851.
21. Li G, Wang Q, Liu Z, *et al.* Research progress of photodynamic active platinum (IV) complexes as antitumor drugs. Journal of Liaocheng University (Natural Science Edition) 2018; 31(2): 21–32.
22. Zhou A. Advances in biopharmaceuticals and biosimilars. Chinese Journal of New Drugs 2017; 26(3): 296–299.
23. Fang Q. Photodynamic therapy for cancer treatment and the new antitumor photosensitizer sinoporphyrin sodium. Chinese Journal of New Drugs 2014; 23(13): 1540–1545.
24. Qin Y, Han Y, Jin H, *et al.* Drug-loaded copper sulfide nanoparticles with high photothermal conversion and pH-stimuli response for drug delivery. Chinese Science Bulletin 2020; 65(Z1): 203–212.
25. Liu H, Yang Q, Guo W, *et al.* $CoWO_{4-x}$-based nanoplatform for multimode imaging and enhanced photothermal/photodynamic therapy. Chemical Engineering Journal 2020; 385: 123979.
26. Li J, Peng Q, Wang L, *et al.* pH- and NIR laser dual-responsive metal-organic frameworks ZIF–8 with MoS_2 nanosheets and DOX loading for chemo/photothermal synergistic cancer therapy. Acta Laser Biology Sinica 2019; 28(5): 421–430.